International Journal of Rock Mechanics & Mining Sciences 143 (2021) 104785

Contents lists available at ScienceDirect

International Journal of Rock Mechanics and Mining Sciences

journal homepage: www.elsevier.com/locate/ijrmms

Size effect and other effects on mode I fracture toughness using two testing methods

Andrea Muñoz-Ibáñez *, Jordi Delgado-Martín, Ricardo Juncosa-Rivera

School of Civil Engineering, University of A Coruña, Campus de Elviña s/n, 15071, A Coruña, Spain

A B S T R A C T

Mode I fracture toughness (K_{IC}) is an intrinsic material property that quantifies its resistance to tensile fracture propagation. The International Society for Rock Mechanics has endorsed four methods to determine the K_{IC} of rock, namely, the short rod, chevron bend, cracked chevron notched Brazilian disc, and semi-circular bend (SCB) methods. In this study, we compare the results of the SCB technique with those of the recently proposed pseudo-compact tension (*p*CT) test, which has proven to be convenient for the assessment of K_{IC} in both fragile and ductile rocks. We select the SCB as a benchmark method due to its popularity, simplicity, and straightforward testing configuration. We discuss the results of 146 tests performed with different lithologies (Arcera, Pinacas and Corvio sandstones, and Blanco Mera granite), different sample sizes (100, 50 and 38 mm diameter), and a range of notch lengths. We also assess test repeatability and intercomparability of the results obtained using the two techniques. Compared with the SCB test, the *p*CT test allows for improved control of the specimen behaviour after the peak load, which provides a greater wealth of fracture mechanics information. *p*CT specimens yield results with higher repeatability than SCB samples. Although we observe that K_{IC} tends to decrease with an increase in the notch length ratio, this effect appears to be non-significant based on statistical assessments. Accordingly, the corresponding mean K_{IC} values are comparable for medium- and large specimens. The influence of specimen size is more pronounced in the SCB tests, while the *p*CT tests show less dependence for harder lithologies. Therefore, to set up minimum specimen requirements for fracture toughness testing, in addition to geometrical constraints, some key lithology-dependent properties (strength, mineralogy, grain size, etc.) should also be considered. Further methodological considerations related to test execution are also discussed.

1. Introduction

Fracture toughness (K_C) represents the ability of a material to resist crack initiation and propagation. Although fracture toughness is a strength-related property, the fundamental approaches of fracture mechanics testing require specially conditioned samples in which cracks are geometrically constrained to develop in a prescribed direction (i.e., with a starter notch).[1] Several testing methods with well-defined sample geometries are currently used in rock mechanics to determine mode I fracture toughness (K_{IC}). The International Society for Rock Mechanics (ISRM) endorses four testing methods: the short rod (SR), chevron bend (CB), cracked chevron notched Brazilian disc (CCNBD) and semi-circular bend (SCB) methods.[1–4] Due to the simple sample preparation and straightforward methodology, SCB is perhaps the most popular testing method in rock fracture mechanics. However, recently, Muñoz-Ibáñez et al.[5] introduced the pseudo-compact tension (*p*CT) test as a potential alternative to overcome some of the drawbacks (e.g., large sample size and cumbersome preparation) associated with some of the above-mentioned suggested methods. In their work, the authors indicate some advantages of the *p*CT method, including a) a reduced rock requirement ($B = 0.5D$, where B = specimen thickness and D = specimen diameter), in comparison with the CB ($L = 4D$; L = specimen length) and SR ($L = 1.45D$) tests. Although the sample volume needed for the *p*CT test would be similar to that for the CCNBD test ($B = 0.4D$), the volume would be double if we compare it with the SCB (semicircular with $B > 0.4D$) specimen. Other advantages are the b) simpler sample preparation (straight groove and thin starter notch), in comparison with that of the CB, SR, and CCNBD tests (chevron notch); c) enhanced control of crack propagation, in comparison with CCNBD and SCB tests, in which the post-peak behaviour cannot be recorded; and d) application of pure tensile loading, in comparison with the loadings of the CB (three-point bending), CCNBD (compressive loading) and SCB (three-point bending) tests. In addition, the increased ligament area is also advantageous in the case of coarse-grained rocks and small specimens.

Based on fracture mechanics theory, fracture toughness is an intrinsic material property. Accordingly, its experimental determination should render consistent results irrespective of the geometry of the specimen and the configuration of loading. However, when applied to rocks, the experimentally determined K_{IC} values reported by many authors contradict such generally assumed behaviour. Indeed, significant

* Corresponding author.
E-mail address: andrea.munoz@udc.es (A. Muñoz-Ibáñez).

https://doi.org/10.1016/j.ijrmms.2021.104785
Received 18 March 2020; Received in revised form 18 February 2021; Accepted 21 April 2021
Available online 24 May 2021

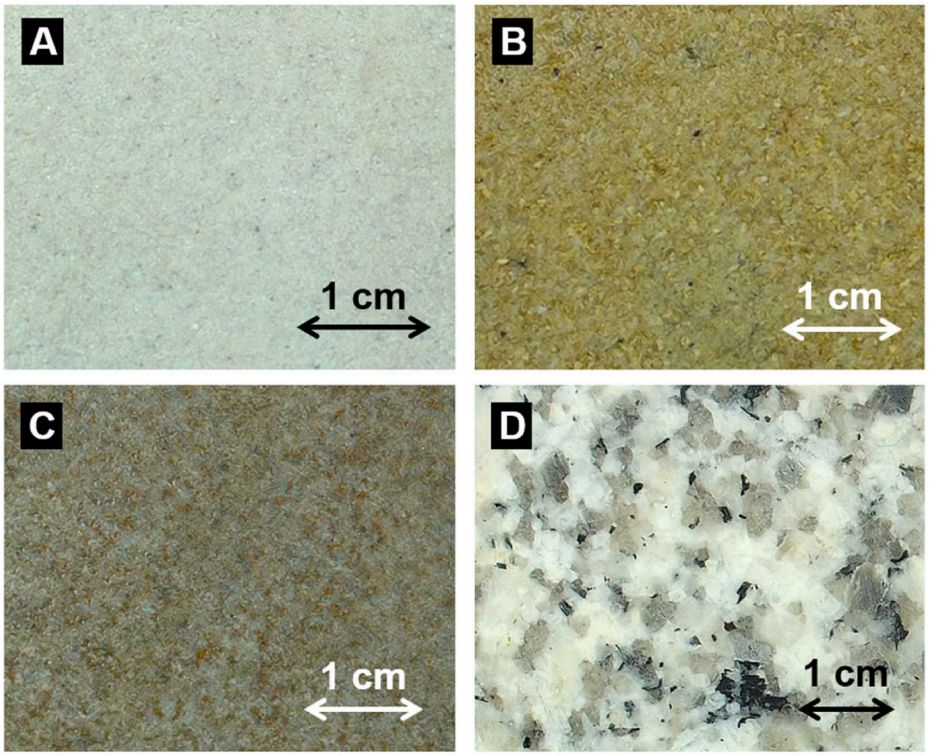

Fig. 1. White light images of the texture and fabric of the four rocks types used in this study: A) Corvio sandstone; B) Arcera sandstone; C) Pinacas sandstone; and D) Blanco Mera granite.

discrepancies in the K_{IC} values can be identified from publications using the same rock type but different testing methods.[6–11] Acknowledging that further experimental efforts are still needed to fill some critical gaps to better understand the variability in the results of fracture toughness testing methods with rocks, in this work, we present the results of 146 K_{IC} determinations performed with four different rock types and the *p*CT and SCB testing approaches. The objective of this study is to determine the consistency of the K_{IC} values obtained using these two methods while taking into account several relevant properties (sample diameter, notch length, and lithology). For each test, we use the corresponding load-displacement curves to characterize the energy content of the fracturing process. In selected tests, we also monitor the acoustic emission (AE) activity. Based on the experimental results, we explore the relationship between the energy release associated with the fracture process and that captured by AE. Finally, we also present some methodological observations related to the SCB testing method.

2. Materials and methods

2.1. Materials

To provide a common ground for the comparison of K_{IC} values derived from the SCB and *p*CT testing methods, we employed four different rock types (Fig. 1): the Corvio (C), Arcera (AR), and Pinacas (PN) sandstones, and Blanco Mera granite (GR) (Sst = sandstone; Grt = granite).

The Corvio sandstone is a coarse-grained quartzarenite from the top section of the Frontada Formation within the stratigraphic Campoo Group (Upper Berriasian, Lower Cretaceous).[12] The Arcera sandstone is a medium-to coarse-grained material included within the Cabuérniga Group (Berriasian-Valanginian, Lower Cretaceous).[13] These two rock types developed within the Basque-Cantabrian Basin in northern Spain, and in both cases, the mineralogy is dominated by quartz (~92%) with less kaolinite (~5%). The grains of these sandstones are cemented by microcrystalline silica and subordinated carbonates.[14,15]

The Pinacas sandstone (also known as Quintanar sandstone) is also a medium-to coarse-grained rock belonging to the stratigraphic Urbion Group (Thitonian-Berriasian, Lower Cretaceous) of the Cameros Basin (Iberian Range, northern Spain). Its mineralogy is dominated by quartz (85–94%) and subordinate amounts of lithic metamorphic fragments (1–3%) and K-feldspar (1–2%).[16] It also incorporates a variable amount (5–8%) of illite.

Corvio, Arcera and Pinacas sandstones are very similar in age (Lower Cretaceous), mineralogy (quartzarenite), texture (well-sorted, ~1 mm diameter subangular to subrounded grains, grain-supported) and paleoenvironment (fluviodetrital), and in fact, they belong to the same sedimentary sequence spread over an area of several hundred kilometres. However, the Pinacas sandstone includes more metamorphic lithic fragments and has been affected by low-grade metamorphism (maximum pressure of ~100 MPa; maximum temperature of ~325 °C), which has led to the conversion of kaolinite into authigenic illite and a more conspicuous presence of silica cement.[17]

The Blanco Mera granite is a 298 ± 5 Ma leucogranodiorite[18] outcropping in the Hombreiro-Santa Eulalia Massif (West Asturian Leonese Zone of the Iberian Massif, NW Spain).[19] Its modal mineralogy is dominated by sericitic plagioclase, K-feldspar and quartz (~35, 27 and 20%, respectively), with significant contents of muscovite (~7%) and biotite (~5%), the last commonly chloritized (~4%). The Blanco Mera granite mineral grain size and shape vary: 1–6 mm allotriomorphic quartz; <6 and up to ~30 mm subidiomorphic plagioclase and K-feldspar; and 1.5 to 2.5 idiomorphic biotite and muscovite.

All the tested rocks are macroscopically homogeneous, but they differ in strength and mechanical performance. Corvio and Arcera sandstones have a relatively low strength, low grain size (~1 mm), high porosity and low elastic moduli. However, the Pinacas sandstone, while having a similar grain size, is significantly tougher and has a lower porosity and higher elastic modulus. In contrast, the Blanco Mera granite is coarser-grained and has a lower porosity. Its strength is moderate compared with other igneous rocks reported in the literature. The properties of these rocks (mineralogy, porosity, uniaxial compressive

Table 1
Selected properties of the rocks used in the study. σ_c = Compressive strength; σ_t = Tensile strength; E = Young's modulus; ν = Poisson's ratio; n_e = Effective porosity. Data for the Corvio Sst (C) is reported in Falcon-Suarez et al. (2017), while data for Arcera Sst (AR), Pinacas Sst (PN), and Blanco Mera Grt (GR) can be found in Muñoz-Ibáñez et al.[5]

Rock	σ_c (MPa)	σ_t (MPa)	E (GPa)	ν	n_e (%)
C	35.4–44.4	1.9–3.1	9.7–19.7	0.3–0.4	18.4–23.5
AR	40.2	4.1–4.9	12.2	0.4	17.3–18.2
PN	129.5	11.2–11.9	35.0	0.2	5.5–6.5
GR	60.4–83.5	9.6–9.7	33.0	0.3	1.2–1.3

strength, indirect tensile strength, ultrasonic velocities, etc.) have been reported in previous studies,[5,14,15,19] and only a short summary is given in Table 1.

2.2. Sample preparation

Fig. 2 shows a schematic diagram of the specimens employed in the SCB and *p*CT tests as well as some relevant reference properties. While the geometry of the SCB specimen is that of a short semicylinder with a single thin notch located at the middle of its flat face, the *p*CT sample is a short full cylinder with a U-shaped groove and a thin notch along its generatrix. The tested samples of the studied rocks were cored from macroscopically homogeneous rock blocks using diamond drill bits to produce plugs 38, 50, and 100 mm in diameter. The plugs were then sliced into discs with a diameter-to-thickness (D/B) ratio of 2. For the SCB specimens, the discs were diametrically halved using a modified tile saw. In this operation, it is essential to guarantee that the cutting plane does not depart by more than 0.2 mm from a diametric plane and remains perpendicular (within less than 0.5°) to the lateral surface of the disc. The last recommendation is key to ensure that the sample can be correctly aligned in the loading fixture afterwards and that the experiments are performed under true mode I conditions. This aspect will be further discussed below. The thin straight notch in the centre of the flat face was cut with a 1 mm-thick diamond disc whose vertical position (which determines the depth of the notch) can be set with the aid of a vertical spindle. Again, it is crucial to ensure the perpendicularity of the notch with respect to the flat surfaces of the specimen to avoid deviations that could degenerate into a mixed tensile/shear fracturing mode. Good alignment of the sample with respect to the saw is ensured with the aid of reference marks (laser level, set square) and the use of a vice fixed to a horizontal movable stand connected to a horizontal spindle.

To systematize the fabrication process, we used 3D-printed fixtures (Fig. 3). In the case of the *p*CT specimens, we used the same notching approach, but we carved the U-shaped groove using a thicker diamond disc (2 mm) and made several parallel saw passes while horizontally moving the sample after each pass (Fig. 3). Then, we cut the thin notch using the same 1 mm-thick disc described for the SCB specimens. The groove and the notch can be made sequentially without removing the sample from the vice. This minimizes eventual deviations and ensures that there is no vertical deviation between them. The samples fabricated according to the previous description were oven-dried at 60 °C for a minimum of 24 h. The reference dimensions of the SCB and *p*CT specimens are reported in Table 2.

To assess the crack mouth opening displacement (CMOD), we used different displacement sensors (Fig. 4). For the SCB tests, a pair of horizontally-laid linear variable differential transducers (LVDTs) and for the *p*CT tests, a crack opening displacement (COD) gauge clipped to a pair of glued steel knife-edge plates. In the case of the SCB test, LVDTs were selected to circumvent the problems inherent to the use of clip-on gauges with small sample sizes. We installed the LVDTs coplanar to the flat face of the sample. However, due to the curved nature of the top surface and the magnification of contact errors associated with the rotation of this surface as the test progresses, we glued 3D printed T-plates to the corresponding edges. Additionally, 6 mm-diameter, 3 mm-thick magnets were glued on the surface of the specimens to hold acoustic emission (AE) sensors.

Although the suggestions of the ISRM consider the use of a minimum sample diameter of 76 mm for SCB testing,[4] to assess the effect of size on K_{IC}, in this study, we also consider larger (100 mm) and smaller sizes (50 and 38 mm). The same scheme was adopted in the *p*CT testing. In addition, we analysed the effect of notch length by testing specimens with a/R (where a = notch length and R = radius of the specimen) and a/b (b = distance from the base of the groove to the bottom of the specimen) ratios of 0.4–0.6 and 0.1–0.4 for the SCB and *p*CT specimens, respectively. However, following different lines of evidence reported by several authors,[20–22] we have not taken into account the effect of variable specimen thickness over K_{IC}, and we have prescribed a constant D/B ratio of 2 for all the experiments.

2.3. Experimental setup

The SCB test was selected due to its simplicity in terms of specimen geometry, sample preparation, loading configuration, and testing procedure.[23] We tested these specimens under three-point bending on a stiff servo-electric frame equipped with a 4,5 kN load cell (Fig. 4A, C). In this configuration, we use an upper steel roller to transfer a linear load to the top of the sample, while two additional lower rollers, separated by a fixed distance (s), support the sample. When testing weak materials, Kuruppu et al.[4] suggest a value for the span-to-diameter ratio (s/D) close to 0.5, while this value increases to 0.8 for stronger materials. Taking into account the varied nature of the tested rocks, we selected a value of s/D of ~0.55 when testing the weaker Arcera and Corvio sandstones, and ~0.65 for the stronger Pinacas sandstone and Blanco Mera granite.

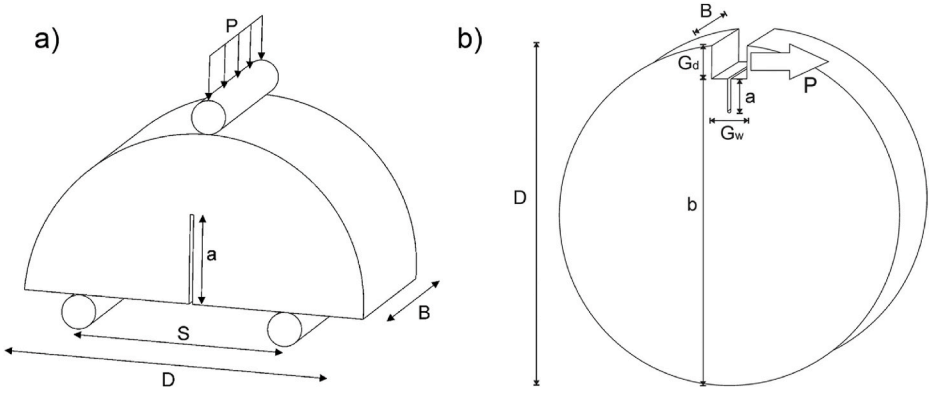

Fig. 2. Schematic illustration of specimen geometries and loading configurations for the SCB (1) and *p*CT (2) specimens. P = applied load; D = diameter; B = thickness; a = notch length; s = span length; G_d = groove depth; G_w = groove width; b = distance from the base of the groove to bottom of the specimen.

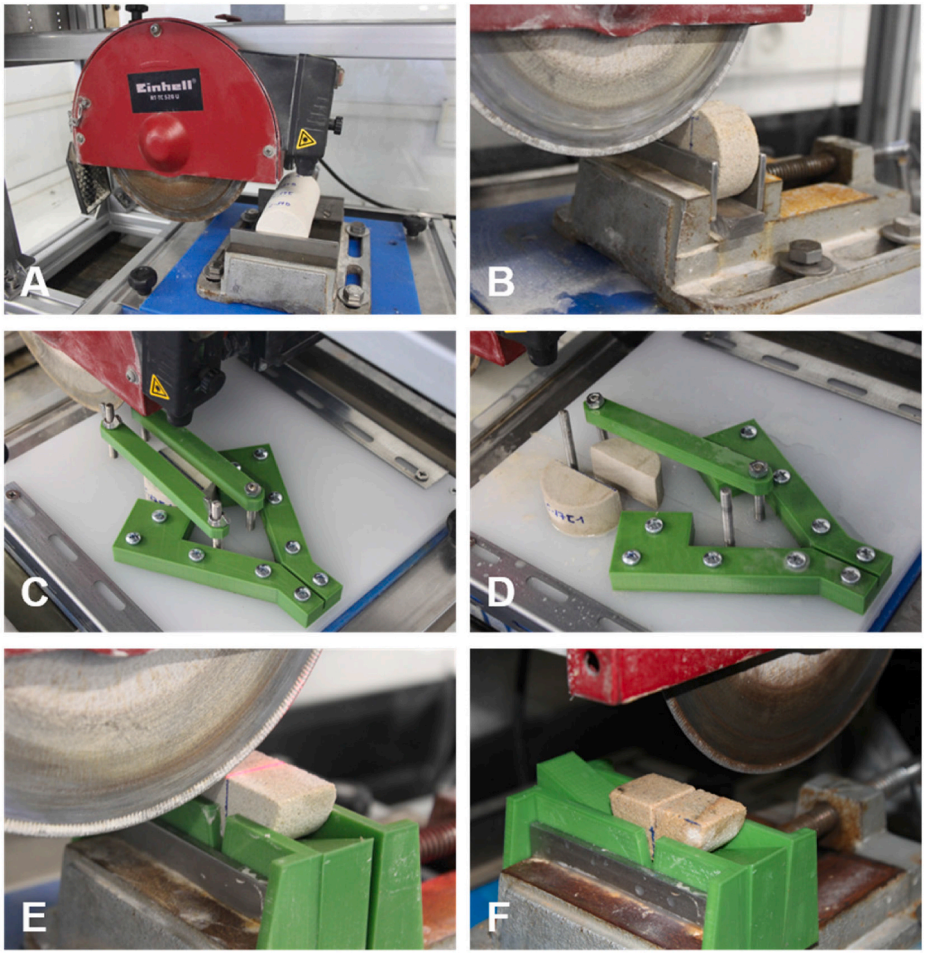

Fig. 3. Preparation of samples for SCB and *p*CT testing. A) Plug slicing; B) U-shaped groove carving; C and D) Halving SCB specimens; E) Laser alignment for straight thin-notch cutting; F) SCB sample finished after a single pass of the diamond saw.

Table 2
Geometrical dimensions of the SCB and *p*CT specimens. D = Diameter; B = Thickness; s/D = span length ratio; a/R = notch length ratio; G_d = U-shaped groove depth; G_w = U-shaped groove width; a/b = notch length ratio.

SBC specimens				*p*CT specimens		
D (mm)	B (mm)	s/D	a/R	G_d (mm)	G_w (mm)	a/b
100	50	0.55–0.65	0.4–0.6	10	10	0.1–0.4
50	25	0.55–0.65	0.4–0.6	5	10	0.1–0.4
38	19	0.55–0.65	0.4–0.6	5	10	0.1–0.4

In the SCB tests, the load point displacement (LPD) corresponds to the vertical displacement of the loading roller, and we assess CMOD using the two LVDTs placed perpendicular to the notch plane and facing each other along the diametric plane of the specimen. The 3D-printed T-plates glued to both sides of the specimen provide flat contact surfaces, and taking into account the magnitude of LPD, it is possible to correct the horizontal displacement for the effect of rotation of the T-plates and obtain an accurate estimate of CMOD. For this testing method, we record the load-CMOD (P-CMOD) and load-displacement (P-LPD) curves for all the specimens.

*p*CT specimens are loaded in pure tension using the specially designed testing device described in detail by Muñoz-Ibáñez et al.,[5] which is equipped with a 50 kN load cell. The specimen is placed on a platform and attached to two steel jaws that penetrate into the U-shaped groove cut in the top of the sample (Fig. 4B, D). With this setup, while one of the jaws remains static, the other jaw is pulled away at a constant displacement rate. Two LVDTs placed symmetrically on both sides of the specimen record the LPD, that is, the displacement of the mobile steel jaw. Furthermore, the CMOD can be determined with the aid of a clip-on gauge mounted on the knife-edge plates glued to the specimen. Because both determinations represent displacements along the same direction, they should render similar results. To check this, a subset of thirteen *p*CT samples included both measurement devices. For both *p*CT and SCB, the experiments were conducted at room temperature and with displacement control at a rate of 0.1 mm/min.

The data reported in the present study have been determined according to Level I testing described in the ISRM suggested methods,[1] that is, including only the value of peak load (P_{max}) in the computations. Kuruppu and Chong[24] consider that this is acceptable in many situations. However, due to the inherent complexity of certain materials such as rocks and other brittle engineering materials (e.g., concrete), we believe that it is advisable to take into consideration the properties considered in Level II testing, especially when more sophisticated non-linear fracture mechanics models are to be applied. Accordingly, we tried to obtain data concerning the post-peak behaviour of the studied rocks by continuing the experiments beyond P_{max}.

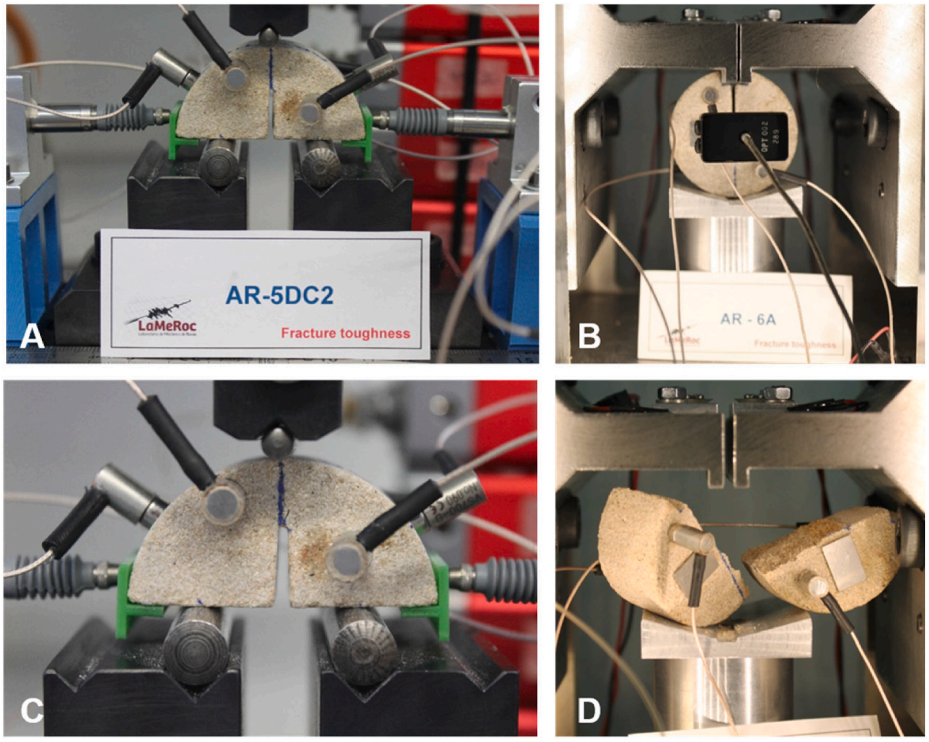

Fig. 4. SCB (left) and *p*CT (right) loading fixtures. The pictures illustrate two samples of 50 mm-diameter corresponding to the Arcera sandstone before (A, B) and after (C, D) the corresponding tests. The SCB samples (A, C) show the disposition of two horizontal displacement transducers (LVDT-type) and the *p*CT (B, D) a crack opening displacement (COD) gauge. The SCB and *p*CT samples illustrated are also equipped with six and four acoustic emission sensors, respectively.

Acoustic emission (AE) is a non-destructive testing technique that can provide interesting insights into the processes of crack initiation, propagation and coalescence. In this respect, we emplaced up to eight miniature Vallen VS700-D AE sensors (6.3 mm-diameter; 10 mm-length) in selected specimens at different distances from the starter notch. Data acquisition was performed with a multichannel AMSY-6 AE system (Vallen Systeme GmbH) equipped with 8 ASIP-2 boards (2 channels per board) with the capability of managing up to sixteen independent signals. We recorded continuous waveforms at a sampling rate of 10 MHz and, to eliminate unwanted frequency components related to environmental or system noise, used a band-pass filter (95–850 kHz) and a signal threshold level of 40 dB. We attached the AE sensors to the samples via 6 mm-diameter, 3 mm-thick magnets that were glued with a thin layer of cyanoacrylate glue (Fig. 4). A thin layer of multi-silicone grease (1110, OKS) was used as the coupling agent at the magnet-sensor interface, providing good acoustic transmission between surfaces.[25] The number of AE sensors employed was four for the *p*CT samples (two on each side of the specimen) and six or eight in the case of the 50- and 100-mm diameter SCB samples. Since it was expected that the cracks would propagate from the notch tip, some of the AE sensors were placed close to the ligament plane.

The raw AE signals were enhanced with Vallen AEP5 preamplifiers with a 34 dB gain. With this AE setup, we recorded a wide number of AE parameters (e.g., counts, amplitude, duration, energy, and frequencies) in real time. However, in this study, we focused on the assessment of AE energy, which is defined as the integral of the squared voltage signal divided by the 10 kΩ reference resistance over the duration of the AE waveform. We recorded the mechanical and AE data separately, so it was necessary to synchronize the records from the two computers involved in data acquisition using a common time stamp.

2.4. Calculations

According to Kuruppu et al.,[4] the computation of mode I fracture toughness (K_{IC}) with the SCB test can be performed based on the following equation:

$$K_{IC}^{SCB} = Y'_{SCB}\frac{P_{\max}\sqrt{\pi a}}{2RB} \tag{1}$$

where $P_{\max}$ is the peak load (in N), a is the notch length (in m), and R and B are the specimen radius and thickness (in mm), respectively. Y'_{SCB} is the non-dimensional stress intensity factor associated with the SCB method, which is given by

$$Y'_{SCB} = -1.297 + 9.516\left(\frac{s}{2R}\right) - \left[0.47 + 16.457\left(\frac{s}{2R}\right)\right]\beta + \left[1.071 + 34.401\left(\frac{s}{2R}\right)\right]\beta^2 \tag{2}$$

in which s is the span length (in mm), and $\beta = a/R$ is the notch length ratio.

In the case of the *p*CT method, and following Muñoz-Ibáñez et al.,[5] K_{IC} is derived as follows:

$$K_{IC}^{pCT} = Y'_{pCT}\,\sigma_{\max}\sqrt{\pi a} \tag{3}$$

where $\sigma_{\max}$ is the applied stress at the critical load ($\sigma_{\max} = P_{\max}/bB$; in Pa). For the computation of the non-dimensional stress intensity factor Y'_{pCT}, these authors provide the following equation, whose coefficients C_i (i = 0 to 4) are given in Table 3.

Table 3
Specimen size-dependent coefficients (C_i) for the computation of the dimensionless stress intensity factor expression corresponding to the *p*CT specimen (Y'_{pCT}).

D (mm)	C_0	C_1	C_2	C_3	C_4
38	10.278	−24.069	82.329	−136.67	127.89
50	12.651	−47.054	158.72	−247.17	185.22
100	15.341	−74.551	260.03	−404.52	273.19

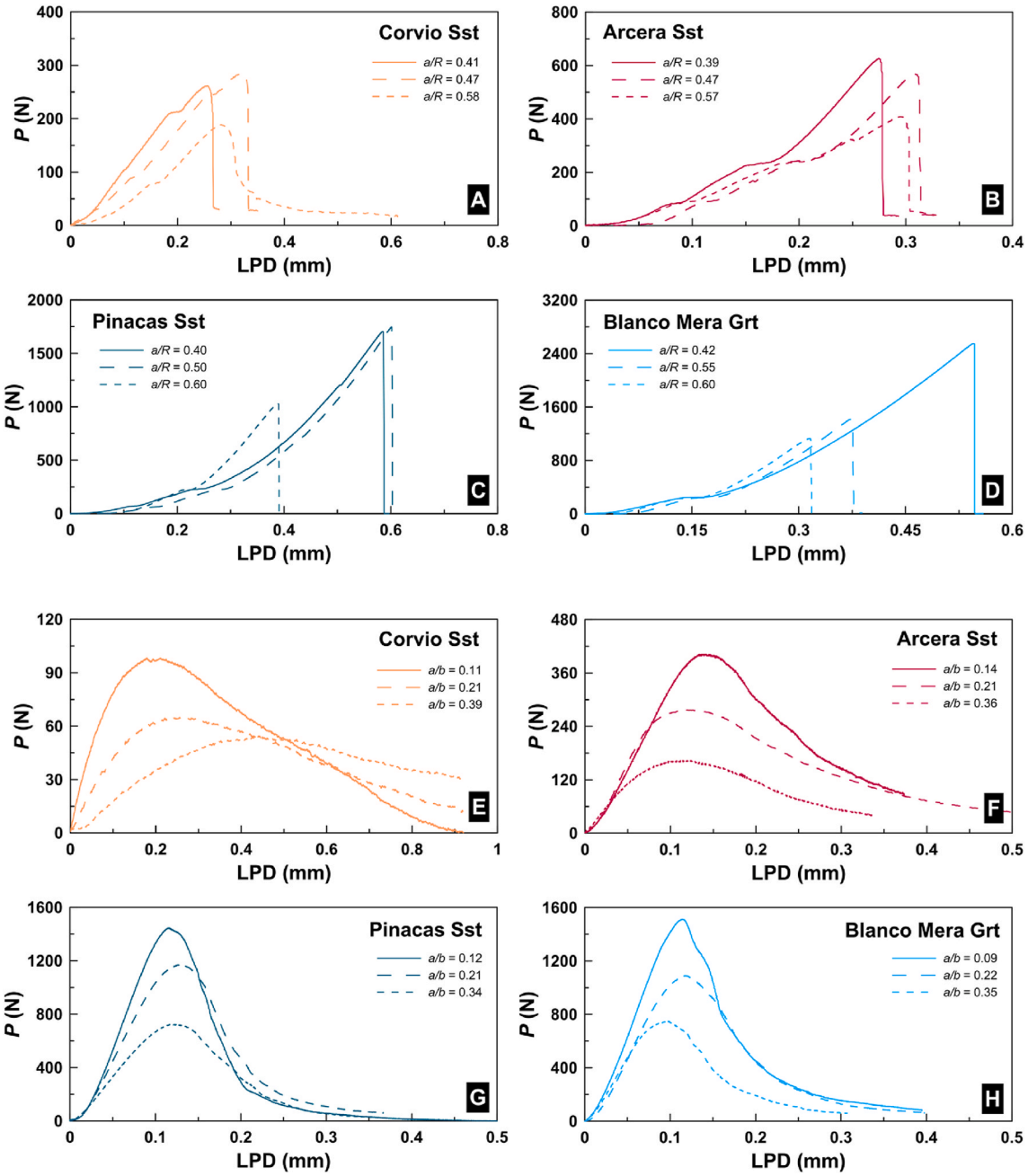

Fig. 5. Load (P) versus load point displacement (LPD) curves obtained for 50 mm-diameter samples tested according with the SCB (A, B, C, D) and pCT (E, F, G, H) methods with different rock samples and notch lengths. See Fig. 1 for notation.

$$Y'_{pCT} = C_0 + C_1\left(\frac{a}{b}\right) + C_2\left(\frac{a}{b}\right)^2 + C_3\left(\frac{a}{b}\right)^3 + C_4\left(\frac{a}{b}\right)^4 \quad (4)$$

The total energy (E_{tot}) was computed by taking the integral over the complete load-displacement (P-LPD) curve as follows:

$$E_{tot} = \int_0^{\infty} P\, d(LPD) \quad (5)$$

To obtain deeper insight into the fracturing process, E_{tot} was split into two contributions: E_{pre} and E_{post} ($E_{tot} = E_{pre} + E_{post}$). E_{pre} represents the pre-peak energy and corresponds to the work done on the specimen to induce the initiation of the crack. E_{pre} is calculated from the integral over the P-LPD curve up to the turning point (P_{max}-d_{peak}, where d_{peak} = displacement at the peak load). E_{post} corresponds to the post-peak energy and represents the work done on the specimen to propagate the crack up to the minimum load threshold value associated with the tail of the P-LPD curve.

3. Results

In the present study, we report the results of 65 and 81 SCB and pCT tests, respectively. Fig. 4 shows representative SCB and pCT specimens before and after the corresponding testing. We observe that the propagation of the fracture generally occurs along the ligament plane, although sometimes it deviates. Following the criterion presented in Kuruppu et al.,[4] some SCB experiments were given a lower confidence when the fracture deviation from the ligament plane exceeded a threshold value of $>0.05D$ (~9.5°–14.0°). In this line, Muñoz-Ibáñez et al.[5] used a threshold deviation angle of 10° for the pCT tests. The results show that crack deviations larger than this threshold affect

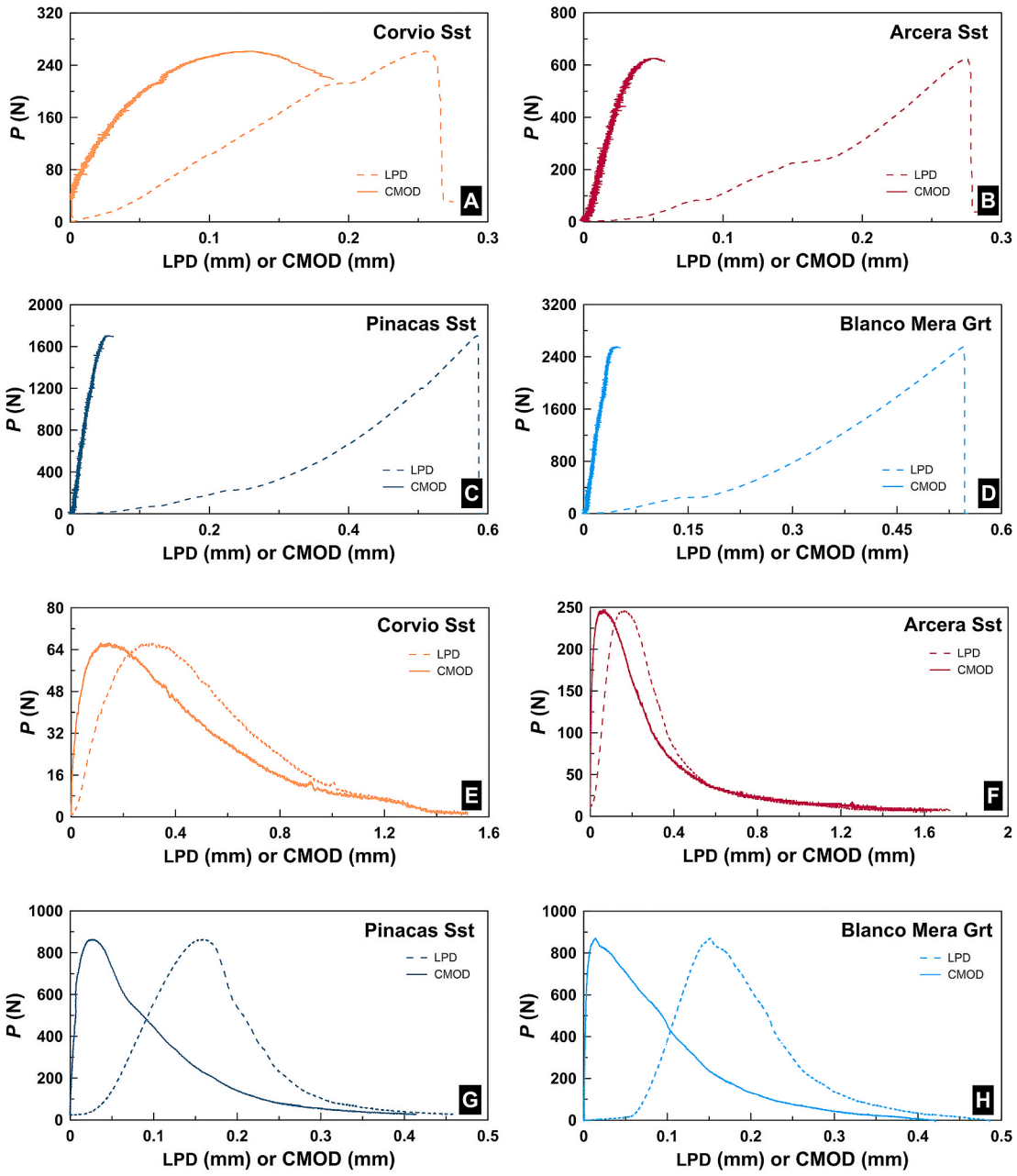

Fig. 6. Load (P) versus load point displacement (LPD) and crack mouth opening displacement (CMOD) curves obtained from 50 mm-diameter samples of different rock types tested according with the SCB (A, B, C, D) and pCT (E, F, G, H) methods. The noth length ratio for all the illustrated experiments is ~0.3–0.4.

~14% of the SCB experiments, and a similar percentage occurs in the pCT case. Although the applicability of this criterion to Level I testing (the peak load is the only experimental property considered) is arguable, it provides a basic screening tool to check the acceptability of tests. In fact, as discussed below, the K_{IC} values considered invalid for deviation of the crack plane in pCT tests even fall in the 95% confidence intervals computed. In the case of the pCT method, an additional ~10% of tests were discarded because of local failures decoupled from the starter notch.

Fig. 5 illustrates some examples of the P-LPD curves for 50 mm-diameter SCB (A to D) and pCT (E to H) specimens as a function of notch length ratio (a/R and a/b, respectively) and rock type. In all the SCB tests performed, the loading curves show a nearly linear increase until the specimen abruptly fails at the peak load (P_{max}). In the SCB tests performed with the sandstones, some of the curves exhibit small loading plateaus that are compatible with local failures that likely occurred at the contact points of the steel rods. With the exception of some specimens of the weak Corvio Sst, it is apparent that the SCB test does not allow good control beyond P_{max}, and the fracture, once initiated, propagates unstably up to the boundaries of the specimen. This behaviour is different with what happens with the pCT specimens, where the P-LPD curves show evidence of good test control in a scenario of slow fracture

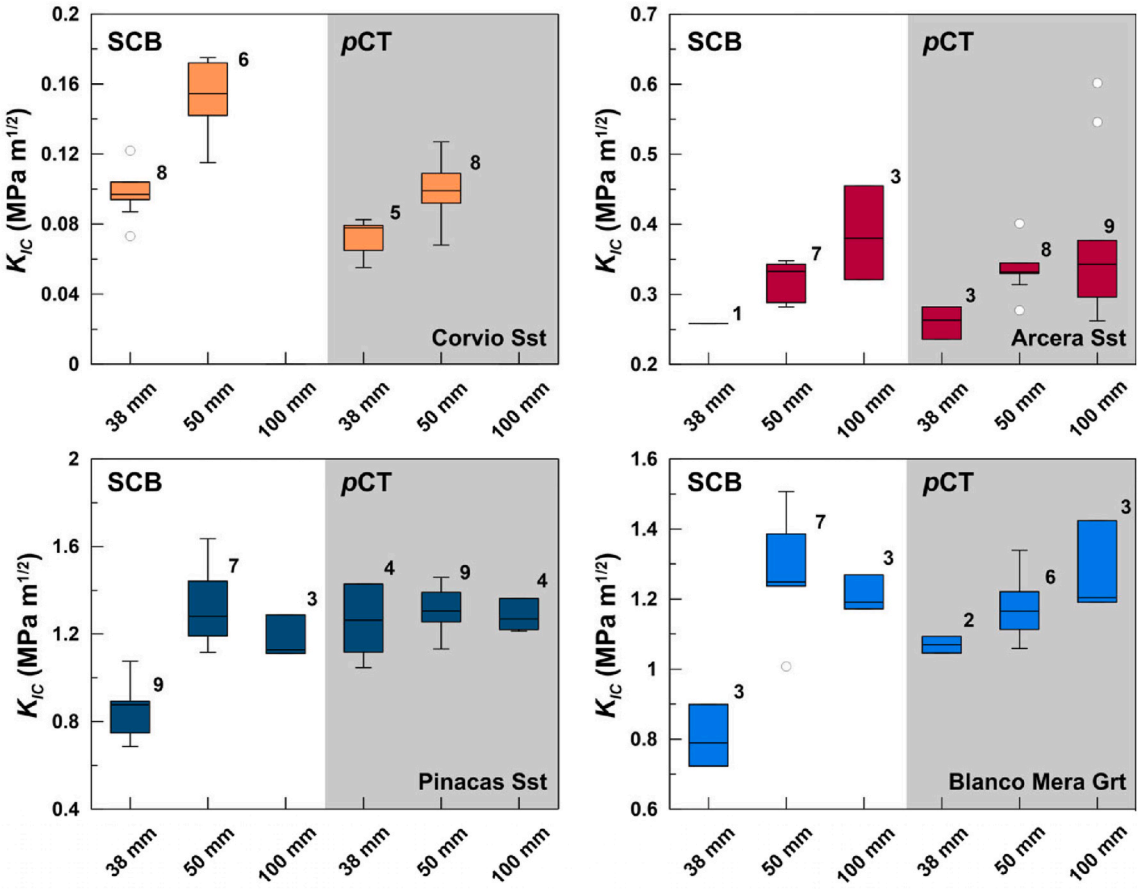

Fig. 7. Box&whisker plots with the aggregated results of the mode I fracture toughness (K_{IC}) tests of rock specimens of different diameter performed with the SCB and *p*CT methods. The number accompanying each group represents the number of samples and single dots correspond to outliers.

propagation after P_{max}.[5] Furthermore, regarding the evolution of P_{max} for different conditions of notch length, there is a systematic trend in the *p*CT results (*i.e.,* P_{max} decreases when the notch becomes longer), but this is not clearly observed in the SCB tests.

Fig. 6 compares some of the *P*-LPD and *P*-CMOD curves obtained for the 50 mm-diameter specimens using the two testing methods. It is worth noting that the magnitude of CMOD in the SCB tests cannot be compared with that of the LPD because these displacements occur in perpendicular directions. However, the measurement of CMOD, as performed in this work, revealed the sliding of the sample along its contact points with the rollers when loaded. In fact, the geometric configuration of the test requires a perfect vertical alignment between the edge of the notch and the loading line. Therefore, unless the load is applied along the vertical radii of the specimen, lateral displacement (and concomitant horizontal sliding) will occur due to the circular nature of the sample. This aspect entails two significant outcomes. First, an inadequate sample preparation (coring, cutting, and notching) and/or careless alignment in the testing jig may induce a mixed mode I/II (tensile/shear) fracture behaviour instead of the expected mode I (tensile) behaviour. Second, in any case, sample misalignment problems may enhance the scattering of results. In this regard, Nsengiyumva and Kim[26] have also reported the great influence that the loading fixtures used to test SCB specimens may have on the energy or peak load results.

Fig. 7 shows a series of box and whisker plots with the aggregated results of K_{IC} obtained for the four reference rock types from the 38-, 50- and 100-mm diameter samples tested with the SCB and *p*CT methods. Overall, the results in both cases are broadly consistent for each tested rock type. However, the 38 mm-diameter samples have lower K_{IC} values, especially in the case of SCB testing (see also Table 4). Apparently, this size effect affects the *p*CT results less than the SCB results and is likely related to the presence of heterogeneities in the tested rocks. For specimens of equal diameter, the smaller ligament area of the samples used in the SCB method makes them more sensitive to this effect.

Table 4
Mode I fracture toughness (K_{IC}) results obtained for the SCB and *p*CT tests performed. Valid tests (see text) are reported for each group of samples within brackets.

Method	Rock	K_{IC} (MPa m$^{1/2}$)		
		D = 38 mm	D = 50 mm	D = 100 mm
SCB	C	0.07–0.12 *(8)*	0.12–0.18 *(6)*	–
	AR	0.26 *(1)*	0.28–0.35 *(7)*	0.32–0.46 *(3)*
	PN	0.69–1.08 *(9)*	1.12–1.64 *(7)*	1.11–1.29 *(3)*
	GR	0.72–0.90 *(3)*	1.01–1.51 *(7)*	1.17–1.27 *(3)*
*p*CT	C	0.06–0.08 *(5)*	0.07–0.12 *(8)*	–
	AR	0.24–0.28 *(3)*	0.28–0.40 *(8)*	0.26–0.60 *(9)*
	PN	1.05–1.43 *(4)*	1.13–1.46 *(9)*	1.21–1.36 *(4)*
	GR	1.05–1.09 *(2)*	1.06–1.34 *(6)*	1.19–1.42 *(3)*

The data in Fig. 7 have been disaggregated in Fig. 8 and are presented as a function of the corresponding notch length ratios (a/R and a/b). In the case of the SCB, it seems that K_{IC} depends on the notch length in hard rocks (Pinacas sandstone and Blanco Mera granite), while this dependence becomes nearly negligible for softer rocks (Arcera and Corvio sandstones). However, it appears that the *p*CT method provides more consistent and sensitive information with respect to this dependence than the SCB. Regarding specimen size, K_{IC} values tend to increase with specimen diameter, although the results are more scattered for smaller samples (D = 38 mm).

The values of E_{tot} computed from the complete *P*-LPD curves are

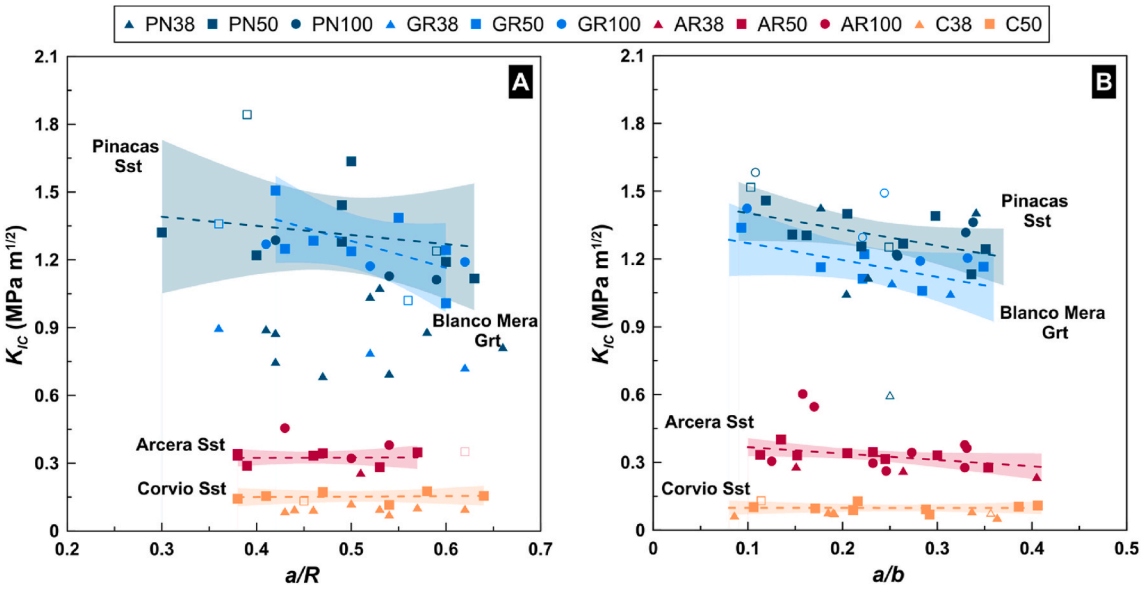

Fig. 8. Mode I fracture toughness (K_{IC}) results from SCB (A) and *p*CT (B) tests as a function of the notch length ratio (a/R or a/b) and diameter of the specimen (triangle = 38 mm; square = 50 mm; circle = 100 mm). Results of assumed higher reliability (fracture deviation <0.05*D* for SCB and <10° for *p*CT; See text) are given with solid symbols while those of lower confidence are illustrated with empty symbols. Dashed lines represent the linear fits computed only with the solid symbols (n = 6 for C; n = 7 for AR, PN, and GR). The shaded areas bound the 95% confidence bands of the corresponding linear fit.

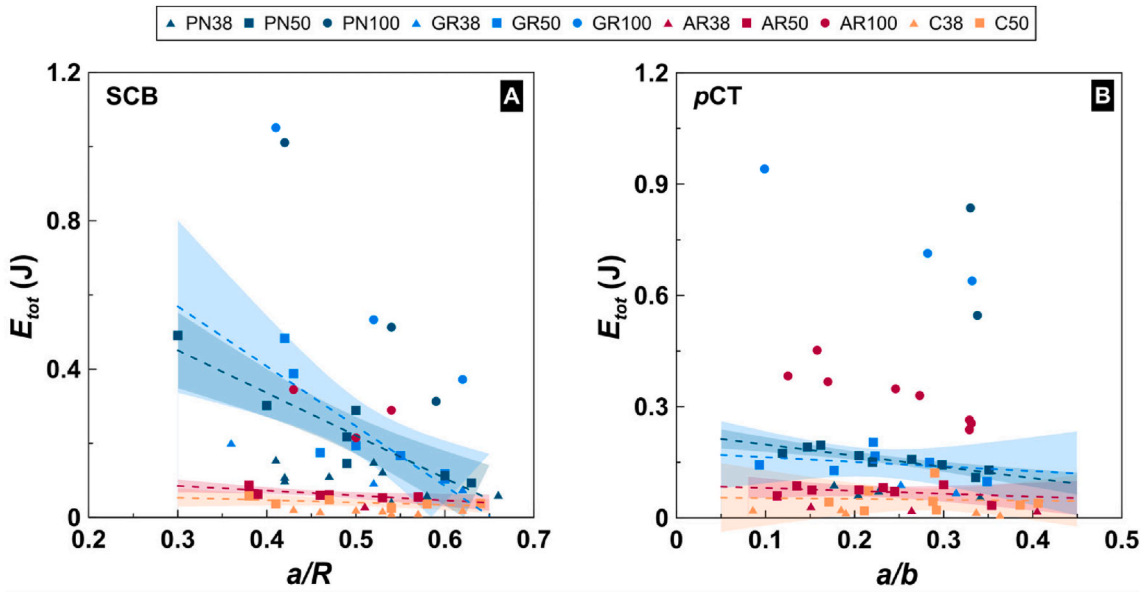

Fig. 9. Total energy (E_{tot}) values associated with SCB (top) and *p*CT methods (bottom) represented as a function of notch length ratios (a/R and a/b, respectively) and specimen diameter (D). Dashed lines represent correlation lines computed for high-confidence results performed with 50 mm-diameter specimens of Corvio (C), Arcera (AR) and Pinacas sandstones (PN), as well as the Blanco Mera granite (GR). The shaded areas shown the confidence intervals (95%) in each case.

represented in Fig. 9 as a function of the notch length ratios and diameter of the SCB and *p*CT specimens. In both cases, E_{tot} is greater when the diameter increases. However, this is more pronounced in the *p*CT tests than in SCB tests, especially for the 100 mm-diameter samples. E_{tot} is also greater for shorter notch lengths, but this effect is more prominent in harder rock types (i.e., PN and GR).

Good control during the execution of the *p*CT tests allows the total energy to be split into two portions: That associated with the *P*-LPD curve up to P_{max} (E_{pre}) and that from P_{max} and beyond (E_{post}). These two portions separate the energy needed to initiate the crack and that required for its unstable propagation. Fig. 10A shows the cross-correlation between pre-peak and post-peak energies for the *p*CT tests of this study. Disregarding the effects of lithology or sample size, E_{post} is ~20% greater than E_{pre}. Due to the configuration of the *p*CT test (LPD and CMOD are measured in the same direction), in this case, it is also possible to compare E_{tot} with the energy computed from the *P*-CMOD curves ($E_{tot,\ CMOD}$; Fig. 10B). Although $E_{tot,\ CMOD}$ is ~17% lower than E_{tot}, the high correlation coefficient (R^2 = 0.99) obtained for a through-origin linear fit suggests that for the *p*CT configuration, it would not be necessary to use special transducers to assess the CMOD, as discussed below. It should be noted that this analysis cannot be performed for the SCB configuration for the following reasons: i) the lack of control of crack propagation prevents the estimation of E_{post}; and ii) in the SCB tests, as mentioned before, CMOD is perpendicular to the load direction,

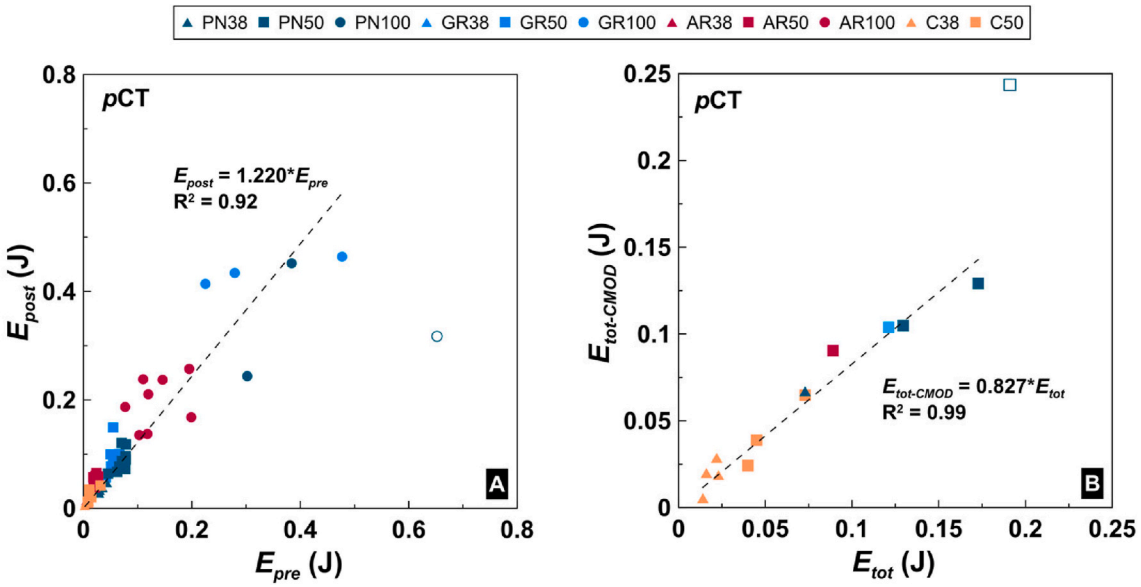

Fig. 10. (A) Cross correlation of the energies before (E_{pre}) and after (E_{post}) peak load); and (B) Total energy computed from *P*-LDP curves (E_{tot}) vs total energy computed from *P*-CMOD curves ($E_{tot,\ CMOD}$). Low confidence results are illustrated with empty symbols.

so E_{tot} and $E_{tot,\ CMOD}$ might not be comparable.

4. Discussion

4.1. Variability in the results associated with the method of testing

The mode I fracture toughness derived from the *p*CT testing of Corvio (~0.06–0.12 MPa $m^{1/2}$) and Arcera sandstones (~0.24–0.60 MPa $m^{1/2}$) are low, which is consistent with their condition of weak rocks. However, the corresponding K_{IC} values of Pinacas sandstone and Blanco Mera granite (~1.05–1.4 MPa $m^{1/2}$) are appreciably higher. For the same rocks, the SCB testing method results in values slightly larger for Corvio Sst (~0.07–0.18 MPa $m^{1/2}$), but lower for Arcera Sst (~0.26–0.46 MPa $m^{1/2}$). In the case of the Pinacas Sst and the Blanco Mera Grt, the K_{IC} results are also more scattered than those derived from the *p*CT testing (~0.69–1.64 and ~0.72–1.51 MPa $m^{1/2}$, respectively). The K_{IC} values obtained from the SCB testing for the Arcera sandstone are of the same magnitude as those of similar rocks tested with the same method.[21] Likewise, the magnitude of the SCB results for the Blanco Mera granite compares well with data reported for igneous rocks in the literature.[27,28]

In a first-order approach, a graphical assessment (e.g., Figs. 7 and 8) is useful for a preliminary inspection of the average similarity or difference of the K_{IC} values obtained with the two testing methods. However, a statistical approach provides sounder quantitative information when considering test repeatability and reproducibility with respect to sample size and testing method. Therefore, we assessed the experimental data with the aid of the free software *Past 3.0*.[29] First, we split the K_{IC} values into 22 separate groups based on the testing method, rock type, and specimen diameter. Then, we performed two subsequent statistical checks: i) a within-group analysis of repeatability (focused on the assessment of normality through a non-parametric Shapiro-Wilk test and the derivation of the corresponding statistical descriptors) and ii) a between-group analysis aimed at the comparison of means (size and testing method effects) based on a one-way analysis of variance (ANOVA) and the non-parametric Mann-Whitney pairwise test. We choose a significance level of 95% ($\alpha = 0.05$) so that the rejection of the null hypothesis (H_0) can be verified if the probability is below this threshold value. For those groups in which we concluded that the means were comparable, representative values of K_{IC} are given (Table 5), as described below.

Table 5
Representative K_{IC} (range in the case of Corvio Sst; mean ± standard error of the mean for the remaining) derived from the statistical analysis for each rock type and testing method. Notes: a) specimens of 38 and 50 mm-diameter; b) specimens of 100 mm-diameter; c) specimens of 50 and 100 mm-diameter; d) specimens of 38, 50, and 100 mm-diameter.

Rock type	K_{IC} (MPa $m^{1/2}$)		
	SCB	*p*CT	All
C	0.07–0.18 (n = 14)[a]	0.06–0.12 (n = 13)[a]	0.06–0.18 (n = 27)
AR	0.39 ± 0.04 (n = 3)[b]	0.33 ± 0.01 (n = 17)[c]	0.36 ± 0.02 (n = 20)
PN	1.27 ± 0.05 (n = 10)[c]	1.33 ± 0.03 (n = 17)[d]	1.31 ± 0.03 (n = 27)
GR	1.25 ± 0.04 (n = 10)[c]	1.21 ± 0.03 (n = 11)[d]	1.23 ± 0.03 (n = 21)

Only three out of the twenty-two groups of data do not conform to a normal distribution (SCB: 50 mm specimens of Arcera Sst; *p*CT: 38 mm specimens of Corvio Sst and 100 mm or Arcera Sst), which is in line with the evidence documented by different authors suggesting that distribution functions of rock mechanics properties are generally normal distributions.[30] Consequently, these groups were not considered in the subsequent stage of mean value comparison.

For the SCB method, the size-dependent reproducibility assessment reveals that the mean values of all the rocks tested cannot be compared for the smaller samples (38 and 50 mm), while it is possible to compare them with the larger samples (50 and 100 mm). Although a similar observation is obtained for the *p*CT method for the weak Corvio and Arcera sandstones, the corresponding means are comparable irrespective of sample size for the strong Pinacas sandstone and Blanco Mera granite. This suggests that no scale effects are apparent in the K_{IC} for these lithologies and sizes.

For each rock type, the testing method reproducibility was determined by combining the groups of specimens whose mean values were proven to be comparable in two datasets (one for SCB and the other for *p*CT). The results show that the average values of the fracture toughness derived from the two methods are consistent as long as the smaller specimens of Arcera Sst for both testing methods and those corresponding to Pinacas Sst and Blanco Mera Grt for the SCB testing are excluded. In the case of Corvio Sst, due to the absence of large specimens, we could not determine the minimum specimen diameter necessary to obtain consistent K_{IC} values between both testing methods. Although mean values are broadly comparable for both testing methods,

we also observe that K_{IC} has lower variability in the case of the *p*CT than in the SCB test, even considering small samples. The previous observations are broadly in agreement with what we can perceive from the graphical analysis.

Different authors have already reported the variability effect induced by employing different testing methods for K_{IC}. For instance, Chang et al.[27] assessed the fracture toughness of Keochang granite and Yeosan marble using four different specimen geometries for the uncracked Brazilian disc test (BDT), CCNBD test, SCB test, and cracked chevron-notched semicircular bend (CCNSCB) test. The K_{IC} values obtained via SCB tests were more scattered and lower than those obtained via the CCNBD, CCNSCB, and BDT configurations, especially for the granite. These findings were further confirmed by the observations of Wei et al.[23] and Xu et al.[31] with Dazhou sandstone specimens using the SCB and CCNBD methods, respectively. Interestingly, in their work, Wei et al.[23] observed consistent K_{IC} results for the SCB and CCNSCB methods (Dazhou sandstone: ~2% difference; Quingdao granite: ~6% difference). Among the reasons that could have favoured such consistency, the authors mention the relative homogeneity of the samples (fine-grain sized), the lack of anisotropy, and the similarities between the testing methods (that reduce the size or boundary effects).

Aliha et al.[7] conducted SCB and centre-cracked Brazilian disc (BD) experiments using Guiting limestone. They report higher K_{IC} values when testing with the SCB method than with the BD method, and they argue that this difference may be related to the contribution of the high-order, non-linear stress terms into the stress field at the crack tip. In a more recent contribution, Aliha et al.[11] investigated the K_{IC} of Harsin marble using the four suggested ISRM methods (CB, SR, CCNBD, and SCB). Their results show a clear sensitivity of the K_{IC} value obtained to the testing method, with SR and CCNBD resulting in the highest and lowest values, respectively. The authors attributed the variability to effects associated with a non-singular T-stress, which is a property that depends on the geometry and loading configuration of the specimen. Conversely, Iqbal and Mohanty[10] reported a negligible discrepancy between K_{IC} values obtained with the CB and CCNBD tests as long as the effects of specimen size and anisotropy are minimized. Tutluoglu and Keles[32] obtained significantly lower K_{IC} values for SCB testing compared to CCNBD when testing the Ankara andesite (~35%) and the Afyon marble (~47%). These authors attribute the difference to the size of the fracture process zone (FPZ) around the crack tip. They conjecture that a larger FPZ compared with sample size (as in the case of the geometry of the SCB specimen) has a greater impact on K_{IC}. Funatsu et al.[33] also reported lower K_{IC} results for SCB specimens when compared to the results of CB and CCNBD specimens of the same rock types. In that case, the authors attributed the variability in the results to differences in the characteristics of the notch type (i.e., chevron or straight-type) and the influence of the FPZ.

To satisfy the conditions for the application of the relationships of linear elastic fracture mechanics (LEFM) and to guarantee a linear elastic behaviour of the material, the size of the FPZ ahead of the crack tip should be small enough compared with the dimensions of the sample. According to Schmidt,[34] the radius of the FPZ (r_{FPZ}) can be assessed as follows:

$$r_{FPZ} = \frac{1}{2\pi}\left(\frac{K_{IC}}{\sigma_t}\right)^2 \tag{6}$$

where σ_t is the tensile strength of the rock. Due to the large number of samples tested in the present study, rather than single-value properties (namely, K_{IC} and σ_t), we considered ranges of values. Accordingly, we computed theoretical minimum (r_{min}) and maximum (r_{max}) radii for the FPZ for each specimen size, lithology and testing method. While we computed r_{min} using the minimum K_{IC} and the maximum value of σ_t, we assessed r_{max} based on the maximum K_{IC} and minimum σ_t. This maximizes the corresponding FPZ lengths. The values resulting from the computations are reported in Table 6. We found that, in general, the size of the FPZ increases with the size of the specimen. This also has been reported by Tarokh et al.[35] With the exception of the Arcera sandstone, for the 50-mm diameter samples, the FPZ is larger in SCB specimens than in *p*CT specimens. For smaller (38 mm) and larger (100 mm) specimen diameters, the trends are opposite. The larger theoretical FPZ associated with the *p*CT specimens should lead to a greater scatter in the K_{IC} results. However, we observed the opposite trend, which suggests that the FPZ would not play a significant role in the *p*CT testing mode. We conjectured that this is associated with the stabilizing role of the larger ligament area of *p*CT specimens compared with the SCB specimens (~3 times). In the case of the SCB results, the greater experimental scattering may be due to the fact that the 38- and 50-mm diameter specimens fall below the minimum size suggested by Kuruppu et al.[4] to satisfy the requirements of LEFM. However, Chang et al.[27] also found a significant dispersion in the experimental results of the SCB method in larger samples ($D = 75$ and 100 mm), which was interpreted as the result of the absence of a starter crack (i.e., pre-cracking) ahead the notch cut in the sample. Since our *p*CT specimens were not pre-cracked (in the previous sense) and still yielded consistent results for the three sample sizes considered, we believe that this is not a critical issue to justify the variability in the data.

Table 6
Estimated size of the FPZ expressed as minimum (r_{min}) and maximum radii (r_{max}), in mm, computed for SCB and *p*CT specimens of different diameter (D).

Method	Rock	$D = 38$ mm		$D = 50$ mm		$D = 100$ mm	
		r_{min} (mm)	r_{max} (mm)	r_{min} (mm)	r_{max} (mm)	r_{min} (mm)	r_{max} (mm)
SCB	C	0.09	0.66	0.22	1.35	–	–
	AR	0.44	0.64	0.53	1.17	0.68	1.96
	PN	0.53	1.47	1.40	3.41	1.39	2.10
	GR	0.88	1.40	1.72	3.92	2.32	2.79
*p*CT	C	0.05	0.30	0.08	0.71	–	–
	AR	0.37	0.75	0.51	1.52	0.46	3.43
	PN	1.23	2.59	1.44	2.70	1.65	2.36
	GR	1.85	2.20	1.90	3.10	2.40	3.50

4.2. Specimen size and notch length effects

Generally, within the bounds of a representative elementary volume, the mechanical properties of rocks derived from experiments should be independent of the specimen size. However, different authors have reported a decrease in certain properties (e.g., unconfined compressive and tensile strengths) when the size of the specimen increases.[36–38] However, fracture toughness has been described to increase with increasing specimen size for quasi-brittle materials, such as rock or concrete.[10,39–41]

Our experimental database allows us to make some observations on the size effects on K_{IC} derived from SCB and *p*CT testing methods. This is illustrated in Fig. 7, where a preliminary inspection reveals a greater size effect associated with the SCB method than with the *p*CT method. As we pointed out earlier, K_{IC} generally increases when the size of the specimen increases. Although the *p*CT results are consistent when considering the range of variability of each size, the largest K_{IC} values correspond to the largest samples (100 mm). This trend also is observed for the SCB specimens of the weak Arcera and Corvio sandstones. However, for the stronger Pinacas sandstone and Blanco Mera granite, the K_{IC} maxima correspond to the intermediate sample size (50 mm) while the minima correspond to the smaller sample size (38 mm). To minimize size effects, the ISRM suggests the use of samples with a minimum diameter greater than 50 mm in CB and SR tests,[1] and that minimum diameter increases to 76 mm in the case of SCB.[4] However, Kataoka and Obara[42] reported that a minimum diameter of 140 mm would be needed to obtain consistent K_{IC} values when using the SCB method. Our findings are in line with the previous contributions, cautioning against the use of small specimens with the SCB test method.

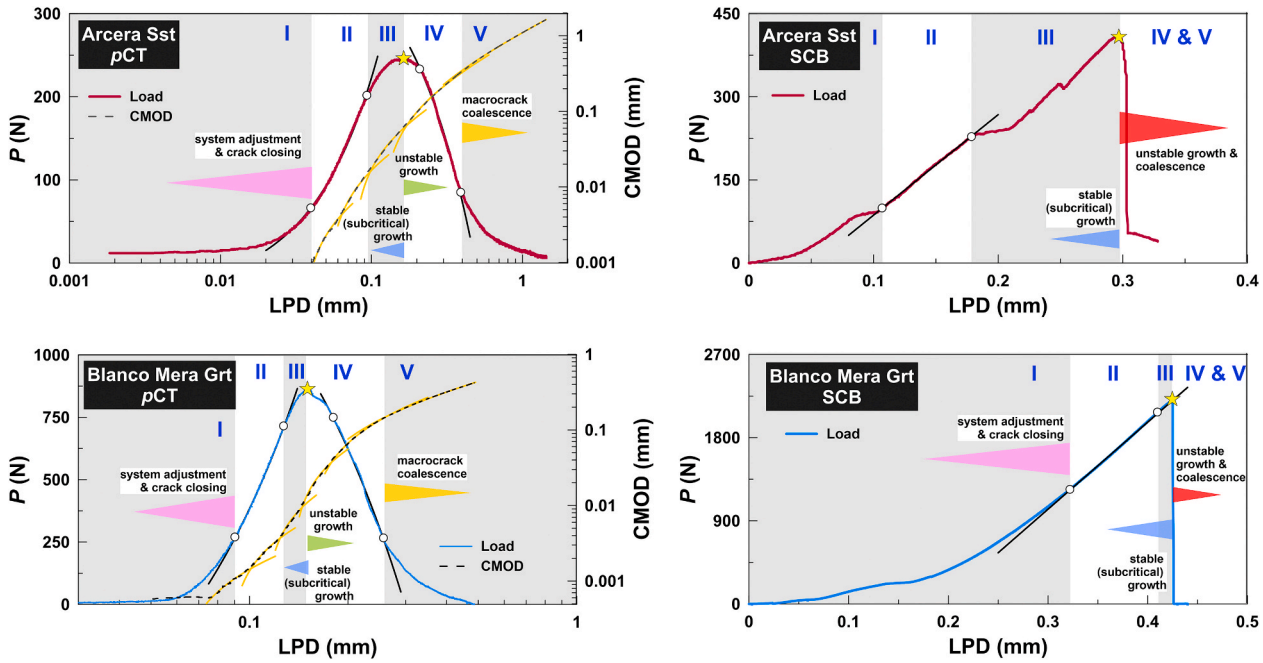

Fig. 11. Identification of the different stages of the failure process in *p*CT (left) and SCB (right) tests for Arcera Sst (top) and Blanco Mera Grt (bottom) specimens. The star symbols identify the peak load, and the empty dots the limits of the linear fittings for the loading curves. The linear fittings for the CMOD vs LPD curves are plotted in yellow. (For interpretation of the references to colour in this figure legend, the reader is referred to the Web version of this article.)

Ueno et al.[39] observed an increase in K_{IC} with increasing SCB specimen diameter (50–100 mm) for Kimachi and Isahaya sandstones. These authors also reported that the FPZ had a greater impact when the specimen was smaller, as seen from the increase in the non-linearity of the *P*-LPD curves close to P_{max}. In our case, the experimental results suggest that the evolution of the slope of the *P*-LPD curves would depend more on the rock type than the size of the specimen. Thus, the weaker materials (Corvio and Arcera Sst) show a greater degree of non-linearity for the three specimen sizes considered in this study. In fact, the statistical analysis has shown a greater dependency of K_{IC} on specimen size for the studied rocks, with populations sometimes not conforming to normal distributions. Lithology seems to change the influence of specimen size on K_{IC}. In our opinion, in addition to geometric constraints, the characteristics of the rock tested must be taken into account to set minimum requirements for specimen size in fracture toughness testing.

The influence of notch length on mode I fracture toughness has been assessed in different studies. Although some authors point out a negligible impact (e.g., Lim et al.[43] and Funatsu et al.[33]), others suggest that K_{IC} tends to decrease as the notch length increases.[44,45] A graphical analysis of our data (see Fig. 8) also supports this conclusion for the *p*CT method and even for the SCB method, despite having used the range of a/R ratios ($0.4 \leq a/R \leq 0.6$) recommended by the ISRM.[4] In addition, the effect seems to be more pronounced for stronger rocks (higher relative K_{IC} values) and almost imperceptible for weaker rocks (lower relative K_{IC} values). To check this conjecture, we performed a second statistical analysis of the data by grouping the K_{IC} values depending on their corresponding notch length. Once more, we considered the significance level of 95% in the within-group analysis and the between-group analysis. In this case, all the groups conformed to normal distributions, and the Mann-Whitney pairwise tests were always successful, suggesting that the dependency of K_{IC} on notch length might not be as determinant as suggested by the plots.

4.3. Stress-strain evolution

The shape of the loading curves incorporates relevant information about the different stages of the fracturing process. Martin and Chandler[46] proposed a model for describing the progressive failure of brittle rocks in compressive tests, which was later adapted to tensile testing.[47] In this study, we follow a similar approach to illustrate the progressive damage process occurring during the SCB and *p*CT tests.

Based on the *p*CT test results (for which we obtain complete loading curves), it is possible to divide the *P*-LPD curves into five (I to V) stages, which are illustrated in Fig. 11 and described as follows: (I) system adjustment and closure of pre-existing cracks, which is characterised by an initial non-linear response; (II) linear elastic deformation; (III) crack initiation and subcritical (stable) crack growth, which would occur when the curve loses linearity, close to P_{max}; (IV) unstable crack growth, as the material progressively losses strength after P_{max} but still preserves some cohesion; and (V) macrocrack coalescence. During stage (III), cracks propagate stably, mainly because of their isolation. However, as mesocracks (which may extend beyond grain boundaries) start to interact, the damage process is accelerated, and macrocracks form. In Fig. 11, the transition between stages (I) and (II) occurs at lower LPD values for the granite than for the sandstone. This could be related to a lower density of pre-existing cracks or different geometrical features.[48] Similarly, shorter stages of stable and unstable crack growth correspond to the granite, which may indicate that the development of microcracks has a deeper impact in decreasing the overall resistance for this rock material.

Regarding the evolution of the CMOD, we observe that, for the same test, P_{max} occurs at CMOD levels lower than the LPD. This discrepancy could be related to geometrical factors: while LPD is measured along the loading line, CMOD is measured close to the original notch tip. However, it seems that lithology may play an additional role, since the difference is more pronounced for harder rock types. In fact, the *P*-LPD and *P*-CMOD curves for the Pinacas Sst and Blanco Mera Grt show larger discrepancies than those for softer rocks (Fig. 6). For the Arcera Sst, the slope of the *P*-CMOD curve is nearly constant from the beginning of the elastic stage, with small variations mainly coinciding with the transitions between stages (as seen from the change in the slope of the CMOD-LPD curve). In fact, the correlation between CMOD and LPD is ~1 ($R^2 = 0.99$), which suggests that it would not be necessary to use clip gauges or other transducers to measure the CMOD. In contrast, the differences are larger

Table 7
Coefficients representing the partial contribution of the pre-peak (a) and post-peak (b) energies to the total energy ($E_{tot} = a^*E_{pre} + b^*E_{post}$) for pCT tests.

Rock	D = 38 mm		D = 50 mm		D = 100 mm	
	a	b	a	b	a	b
C	0.34	0.66	0.34	0.66	–	–
AR	0.31	0.69	0.29	0.71	0.45	0.55
PN	0.49	0.51	0.51	0.49	0.56	0.44
GR	0.33	0.67	0.37	0.63	0.42	0.48

for the specimens of Blanco Mera Grt. For this harder rock type, the rate of change in CMOD is lower during the linear elastic stage and increases close to the peak load. In this case, the slope of the CMOD-LPD curve varies between ~0.01–0.15 (R^2 = 0.7–0.8) in the pre-peak region and then increases up to ~1.2 (R^2 = 0.99). This means that CMOD could also be computed from LPD using a correction factor that would depend on the stage of testing.

Although we have also identified stages (I) to (III) during the SCB tests, the lack of control in the post-peak region (crack growth velocity controls the propagation process at P_{max}, and failure occurs immediately thereafter) prevents accurate identification of the boundary between stages (IV) and (V). As mentioned above, the LPD and CMOD cannot be compared for this testing method because these displacements are not measured in the same direction.

4.4. Energy assessment

In fracture mechanics, a crack grows when the stress intensity factor (K_I) reaches a critical value, which is referred to as the fracture toughness (K_{IC}) of the corresponding material.[49] From the point of view of energy balances, a crack will propagate when the energy available for crack growth exceeds the resistance of the material.[50] Accordingly, fracture toughness can also be regarded as the energy release rate needed to create new crack surfaces, that is, two surfaces per crack tip.[1] This energy can be accounted for by computing the surface under the experimental P-LPD curves that formally corresponds to the E_{tot} described with Equation (5). From the beginning of a test up to the point of failure (where the crack starts to propagate), the energy delivered by the testing device mainly goes to subcritical crack growth[51] while approaching K_{IC}. Depending on the methodology, a fraction of this energy can be elastically stored in the sample, and under ideal testing conditions, elastic storage will occur in a small volume of the sample around the starter notch. Once K_{IC} is reached, the energy delivered is then consumed to stably propagate the crack. In a test with satisfactory control, it is possible to obtain a continuous P-LPD curve, allowing us to split the total energy (E_{tot}) into the two above-mentioned stages, which we refer to as E_{pre} and E_{post}. However, the geometry of the tested specimen and the way in which the load is applied determine the success in obtaining a complete curve. In this respect, it is apparent that the pCT method provides good control of the process, while the SCB does not. It can be argued that improving control electronics and system stiffness (to avoid elastic energy storage in the testing device) may improve the quality of SCB results.

However, in our opinion, the key point determining the poorer performance of SCB tests in the post-peak region is that the energy storage in the sample takes place in a volume significantly larger than the near-tip region of the crack (e.g., at the contact point of the rollers and along the ligament up to the starter notch). When the load reaches P_{max}, all this energy stored in the sample is released suddenly, and the crack propagates unstably. However, in the case of the pCT test, the load is transferred to the sample along the contact lines of the pulling jaws[5] and then directly to the starter notch.

Although the relationship between E_{pre} and E_{post} from the pCT test results (Fig. 10A) suggests that the specific energy required to initiate the fracture is ~20% lower than that needed to propagate it, further insights can be gained by considering factors such as lithology and sample size. Considering the relationship of $E_{tot} = a^*E_{pre} + b^*E_{post}$, the coefficients a and b would represent the partial contribution of each portion to the total energy. We computed a and b for each pCT test performed in this study. The average values of both coefficients are compiled for each rock type and specimen diameter in Table 7. The results suggest that for small and intermediate-sized specimens, the specific energy needed to propagate the fracture is double than that required to initiate it. For larger samples, the energy balance is more equilibrated, and E_{pre} is almost equal to E_{post}. Curiously, this is the behaviour observed for all the specimens of Pinacas sandstone, irrespective of the specimen size. We conjecture that this effect could be related to the size of the FPZ with respect to the ligament length or to the degree of cementation of the rock. However, the reason for this finding remains unknown, and more work is needed before any conclusions can be drawn.

Zhang et al.[44] performed SCB tests to characterize the fracture properties of some stabilized soils. They found that ligament area-normalized fracture energy ($E_{tot}/[(R-a)\cdot B]$) tends to decrease as the notch length increases, and a similar tendency has been reported by Rivera-Perez[45] when computing E_{tot} based on the Illinois flexibility index test (I-FIT), which is an adaptation of the SCB test for asphalt

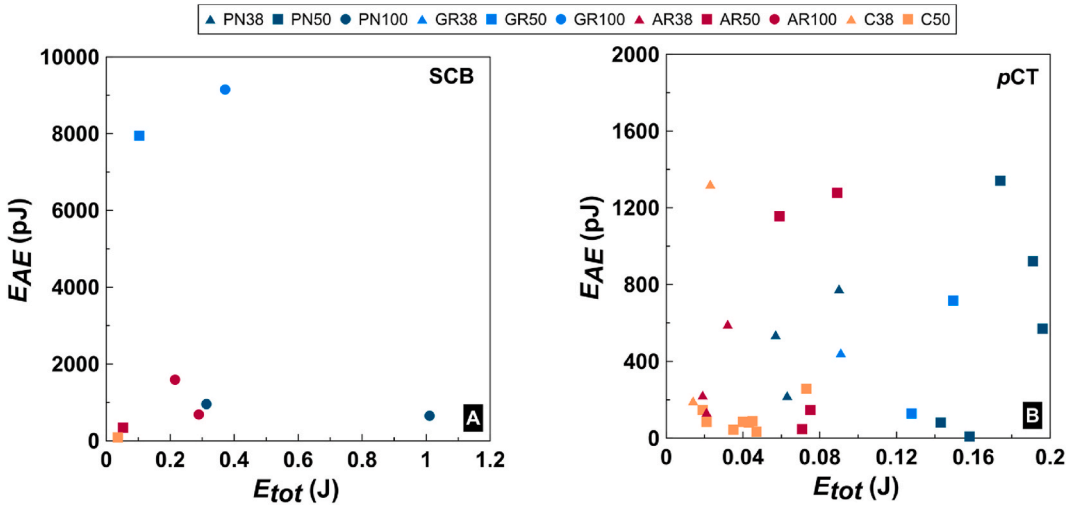

Fig. 12. Total energy (E_{tot}) versus with respect to sample diameter (D) for a range of notch-length ratios 0.2–0.35 and the different rock types tested.

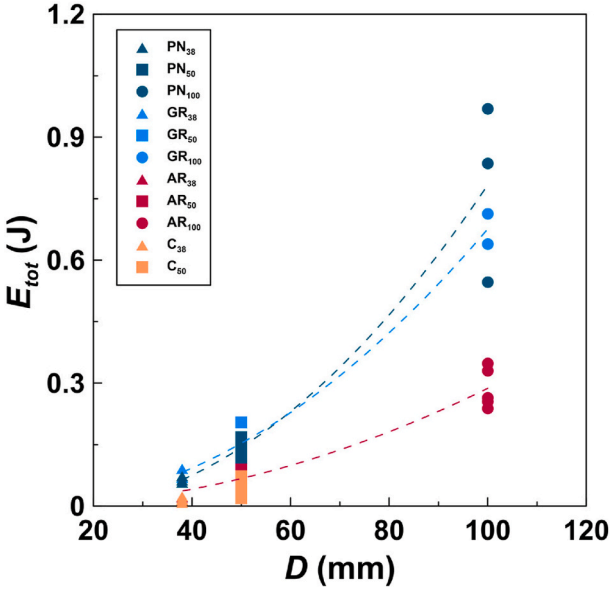

Fig. 13. Total energy (E_{tot}) versus acoustic emission energy (E_{AE}) associated with tests performed with the SCB (A) and *p*CT (B) testing methods in which AE activity was monitored (9 and 28 tests, respectively).

materials. Our results, illustrated in Fig. 9, are consistent with the observations made by the mentioned authors: less clearly in the SCB tests and more in the *p*CT tests. Rivera-Perez[45] attributed this effect to the reduction in the ligament area available for fracture propagation. Thus, for a constant notch length, the change in the size of the specimen should result in a quadratic distribution of E_{tot}. We validate this assumption by plotting E_{tot} vs. D in Fig. 12 for notch ratios (a/b) between 0.2 and 0.35: the best fit that can be obtained is quadratic, which implies a non-constant rate of change. Notably, this relationship appears to be a function of lithology, which is also observed from the slopes of E_{tot} vs. a/b in Fig. 9.

4.5. Acoustic emission energy

According to Landis and Baillon,[52] a certain fraction of the energy evolved during crack generation and propagation can be monitored by taking advantage of AE techniques. Although the energy magnitudes associated with fracturing and local AE are broadly different (AE can be unevenly scattered and/or attenuated in the sample and interfaces), it may be possible to identify a formal relationship between these properties so that AE energy can be regarded as a proxy for the energy dissipated during the fracture process. In fact, considering that the AE activity is proportional to the number and magnitude of growing cracks, it is reasonable to assume that there might be a relation between AE energy (E_{AE}) and fracture energy. Published results are, however, contradictory. For instance, Landis and Baillon[52] reported a good correlation between E_{AE} and fracture energy for mortar specimens, although they could not provide a functional relationship. In contrast, their results show no clear correlation in the case of concrete specimens. On the other hand, Han et al.[53] observed a linear correlation between both parameters in three-point bending tests performed on samples of crumb rubber concrete.

The values of the total emitted E_{AE} obtained at the end of the SCB and *p*CT tests where such measurements are available (9 and 28 tests, respectively), are plotted as a function of E_{tot} in Fig. 13. For this purpose, E_{AE} is taken as the average value from all the AE transducers installed in the sample after summing the AE energy released for each AE event. No clear relationship arises from the plots in either the SCB or the *p*CT tests. In addition, it is worth noting that there is no direct correlation between E_{AE} and the specimen size. However, we believe that more work needs to be done in this line and we cannot discard non-apparent correlations that are not manifested from the available database.

5. Conclusions

We experimentally investigated the mode I fracture toughness (K_{IC}) of three sedimentary rocks (Arcera, Pinacas and Corvio sandstones) and one igneous rock (Blanco Mera granite) by means of two different testing methods: the ISRM-suggested SCB method and the *p*CT technique. From this study, the following conclusions were drawn:

- The *p*CT method provides good test control, even in the post-peak region, making access to level II testing feasible. With this method, the fracture propagation is slow, providing a greater wealth of fracture mechanics information, such as the crack evolution (stable/unstable growth and macrocrack coalescence).
- The SCB configuration is prone to significant elastic energy storage and sudden release at the critical stress, leading to fast and dynamic fracture propagation at failure.
- *p*CT specimens yield more consistent (lower variability) fracture toughness values than the SCB specimens do. The mean K_{IC} values obtained with the SCB and *p*CT configurations are comparable for medium (50 mm) and large (100 mm) samples.
- The influence of specimen size on K_{IC} is more pronounced in the SCB tests than in the *p*CT tests, although the effect is influenced by the rock type. In the *p*CT test, even small (38 mm) samples provide consistent K_{IC} values for the harder lithologies, suggesting higher non-dependency on the specimen size.
- The K_{IC} results can be considered consistent for the notch length ratios considered in this study. In fact, in the case of SCB testing, the variability induced by changing the notch length ratio (a/R) is of less importance than the effect of sample size.
- In *p*CT tests, the good correlation found between LPD and CMOD makes possible the assessment of CMOD without employing direct-contact transducers (clip gauges or similar), which is advantageous for investigating small samples.
- The analysis of the fracture energy reveals that the energy needed to initiate the fracture in *p*CT tests is lower than that required to propagate it along the ligament plane. However, the values are more equilibrated for larger samples.
- The energy balances obtained support the supposition of a size-dependent fracture energy given a constant notch length. However,

our results indicate more complex dependencies, with lithology playing a significant role.
- No relationship between AE energy (E_{AE}) and fracture energy could be established in the present survey, and a more comprehensive AE database is needed.

From a methodological point of view, good sample alignment is essential in the SCB method to avoid mixed modes (I/II) in fracture toughness determinations. Furthermore, we also caution about the propensity of this configuration to lateral sliding when applying a linearly distributed force due to the circular nature of the loading surface. Neither of these problems is significant when utilising the *p*CT technique.

Declaration of competing interest

The authors declare that they have no known competing financial interests or personal relationships that could have appeared to influence the work reported in this paper.

Acknowledgements

This work was funded by Repsol S.A. and supported by the Xunta de Galicia, the European Union (European Social Fund - ESF) and the MINECO/AEI/FEDER EU project BIA2017-87066-R. Funding for open access charge: Universidade da Coruña/CISUG. This contribution has benefited from the discussions and feedback provided by Drs. J. Alvarellos-Iglesias, J. Canal-Vila, N. A. González-Molano and H. J. González-Pérez.

References

1 ISRM Testing Commission. Suggested methods for determining the fracture toughness of rock. *Int J Rock Mech Min Sci Geomech Abstr*. 1988;25(2):71–96.
2 Ouchterlony F, Al M. In: *Fracture Toughness Testing of Rock with Core Based Specimens, the Development of an ISRM Standard*. Fract Toughness Fract Energy. Published online; 1989:231–251. https://doi.org/10.1016/0013-7944(90)90214-2.
3 Fowell RJ, Hudson JA, Xu C, Chen JF. Suggested method for determining mode-I fracture-toughness using cracked chevron-notched Brazilian disc (CCNBD) specimens. *Int J Rock Mech Min Sci Geomech Abstr*. 1995;32(1):57–64.
4 Kuruppu MD, Obara Y, Ayatollahi MR, Chong KP, Funatsu T. ISRM-suggested method for determining the mode I static fracture toughness using semi-circular bend specimen. *Rock Mech Rock Eng*. 2014;47(1):267–274. https://doi.org/10.1007/s00603-013-0422-7.
5 Muñoz-Ibáñez A, Delgado-Martín J, Costas M, Rabuñal-Dopico J, Alvarellos-Iglesias J, Canal-Vila J. Pure mode I fracture toughness determination in rocks using a pseudo-compact tension (pCT) test approach. *Rock Mech Rock Eng*. 2020;53:3267–3285. https://doi.org/10.1007/s00603-020-02102-6. Published online.
6 Alkiliçgil C. *Development of Specimen Geometries for Mode I Fracture Toughness Testing with Disc Type Rock Specimens*. 2010. Published online.
7 Aliha MRM, Sistaninia M, Smith DJ, Pavier MJ, Ayatollahi MR. Geometry effects and statistical analysis of mode I fracture in guiting limestone. *Int J Rock Mech Min Sci*. 2012;51:128–135. https://doi.org/10.1016/j.ijrmms.2012.01.017.
8 Kataoka M, Yoshioka S, Cho S-H, Soucek K, Vavro L, Obara Y. Estimation of fracture toughness of sandstone by three testing methods. In: *Vietrock2015: An ISRM Specialized Conference*. vols. 12–13. Hanoi, Vietnam: March.; 2015.
9 Erarslan N. The importance of testing method to evaluate the most representative mode I fracture toughness value of brittle rocks. *MOJ Civ Eng*. 2018;4(5):437–441. https://doi.org/10.15406/mojce.2018.04.00141.
10 Iqbal MJ, Mohanty B. Experimental calibration of ISRM suggested fracture toughness measurement techniques in selected brittle rocks. *Rock Mech Rock Eng*. 2007;40(5):453–475. https://doi.org/10.1007/s00603-006-0107-6.
11 Aliha MRM, Mahdavi E, Ayatollahi MR. The influence of specimen type on tensile fracture toughness of rock materials. *Pure Appl Geophys*. 2017;174(3):1237–1253. https://doi.org/10.1007/s00024-016-1458-x.
12 García de Cortázar A, Pujalte V. Litoestratigrafía y facies del grupo Cabuerniga (Malm-Valanginiense inferior?) al S de Cantabria-NE de Palaencia. *Cuad Geol Iber*. 1982;8:5–21.
13 Pujalte Navarro V, Robles Orozco S, Hernández JM. La sedimentación continental del Grupo Campóo (Malm-Cretácko basal de Cantabria, Burgos y Palencia): testimonio de un reajuste hidrográfko al inicio de una fase rif. *J Iber Geol - An Int Publ Earth Sci*. 1996;21(21):227–252. https://doi.org/10.5209/rev_CGIB.1996.v21.2530.
14 Canal-Vila J. *Experimental Study of Effect of CO_2 Injection on Rocks: Coupling Hydrodynamic, Mechanical and Geochemical Processesrim*. 2016. Published online.
15 Falcon-Suarez I, Canal-Vila J, Delgado-Martin J, North L, Best A. Characterisation and multifaceted anisotropy assessment of Corvio sandstone for geological CO_2 storage studies. *Geophys Prospect*. 2017;65(5):1293–1311. https://doi.org/10.1111/1365-2478.12469.
16 IGME. Geological Map of Spain at 1/50.000 scale. Memoir of the sheet 316 Quintanar de la Sierra. Published online 1986:52.
17 Casquet C, Galindo Francisco M, González Casado J, et al. El metamorfismo en la Cuenca de los Cameros. Geocronología e implicaciones tectónicas. *Geogaceta*. 1992;11:22–25.
18 Santos-Zalduegui JF, Pin C, Aranguren A, Gil-Ibarguchi JI. Application of specific extraction chromatographic methods to the Rb-Sr, Sm-Nd isotope study of geological samples: the Hombreiro-Santa Eulalia Granite (Lugo, NW Spain). *Geogaceta*. 1996;20(2):495–497.
19 Arzúa J, Alejano LR. Dilation in granite during servo-controlled triaxial strength tests. *Int J Rock Mech Min Sci*. 2013;61:43–56. https://doi.org/10.1016/j.ijrmms.2013.02.007.
20 Kobayashi R, Matsuki K, Otsuka N. 2. Size effect in the fracture toughness of Ogino tuff. *Int J Rock Mech Min Sci*. 1986;23(1):13–18. https://doi.org/10.1016/0148-9062(86)91662-1.
21 Singh RN, Sun GX. An investigation into factors affecting fracture toughness of coal measures sandstones. *J Mines, Met Fuels*. 1990;38(6):111–118.
22 Khan K, Al-Shayea NA. Effect of specimen geometry and testing method on mixed Mode I-II fracture toughness of a limestone rock from Saudi Arabia. *Rock Mech Rock Eng*. 2000;33(3):179–206. https://doi.org/10.1007/s006030070006.
23 Wei MD, Dai F, Xu NW, Zhao T, Xia KW. Experimental and numerical study on the fracture process zone and fracture toughness determination for ISRM-suggested semi-circular bend rock specimen. *Eng Fract Mech*. 2016;154:43–56. https://doi.org/10.1016/j.engfracmech.2016.01.002.
24 Kuruppu MD, Chong KP. Fracture toughness testing of brittle materials using semi-circular bend (SCB) specimen. *Eng Fract Mech*. 2012;91:133–150. https://doi.org/10.1016/j.engfracmech.2012.01.013.
25 ASTM. Standard guide for mounting piezoelectric acoustic emission sensors, E650-97. In: *Annual Book of ASTM Standards*. ASTM International; 1997.
26 Nsengiyumva G, Kim YR. Effect of testing configuration in semi-circular bending fracture of asphalt mixtures: experiments and statistical analyses. *Transport Res Rec*. 2019;2673(5):320–328. https://doi.org/10.1177/0361198119839343.
27 Chang SH, Lee CI, Jeon S. Measurement of rock fracture toughness under modes I and II and mixed-mode conditions by using disc-type specimens. *Eng Geol*. 2002;66(1-2):79–97. https://doi.org/10.1016/S0013-7952(02)00033-9.
28 Donovan JG, Karfakis MG. Adaptation of a simple wedge test for the rapid determination of mode I fracture toughness and the assessment of relative fracture resistance. *Int J Rock Mech Min Sci*. 2004;41(4):695–701. https://doi.org/10.1016/j.ijrmms.2004.01.001.
29 Hammer Ø. PAST PAleontological STatics Reference Manual. *Natular Hist Museum*. 2011;(1999):248.
30 Gill DE, Corthésy R, Leite MH. Determining the minimal number of specimens for laboratory testing of rock properties. *Eng Geol*. 2005;78:29–51. https://doi.org/10.1016/j.enggeo.2004.10.005.
31 Xu Y, Dai F, Zhao T, wen Xu N, Liu Y. Fracture toughness determination of cracked chevron notched Brazilian disc rock specimen via griffith energy criterion incorporating realistic fracture profiles. *Rock Mech Rock Eng*. 2016;49(8):3083–3093. https://doi.org/10.1007/s00603-016-0978-0.
32 Tutluoglu L, Keles C. Mode I fracture toughness determination with straight notched disk bending method. *Int J Rock Mech Min Sci*. 2011;48(8):1248–1261. https://doi.org/10.1016/j.ijrmms.2011.09.019.
33 Funatsu T, Shimizu N, Kuruppu M, Matsui K. Evaluation of mode I fracture toughness assisted by the numerical determination of K-resistance. *Rock Mech Rock Eng*. 2015;48(1):143–157. https://doi.org/10.1007/s00603-014-0550-8.
34 Schmidt RA. A microcrack model and its significance to hydraulic fracturing and fracture toughness testing. In: *The 21st U.S. Symposium on Rock Mechanics (USRMS), 27-30 May*. Missouri.: Rolla; 1980.
35 Tarokh A, Makhnenko RY, Fakhimi A, Labuz JF. Scaling of the fracture process zone in rock. *Int J Fract*. 2017;204(2):191–204. https://doi.org/10.1007/s10704-016-0172-0.
36 Hoek E, Brown ET. *Underground Excavations in Rock*. London: Transactions of the Institution of Mining and Metallurgy; 1980.
37 Klanphumeesri S. *Direct Tension Testing of Rock Specimens*. 2010. Published online.
38 Quiñones J, Arzúa J, Alejano LR, García-Bastante F, Mas Ivars D, Walton G. Analysis of size effects on the geomechanical parameters of intact granite samples under unconfined conditions. *Acta Geotech*. 2017;12(6):1229–1242. https://doi.org/10.1007/s11440-017-0531-7.
39 Ueno K, Funatsu T, Shimada H, Sasaoka T, Matsui K. Effect of specimen size on mode I fracture toughness by SCB test. In: *The 11th International Conference on Mining, Materials and Petroleum Engineering; the 7th International Conference on Mining, Materials and Petroleum Engineering*. vol. 11. Thailand: Chiang Mai; November. ; 2013:13.
40 Brevik NØ. *Experimental Study of Fracture Toughness in Sedimentary Rocks*. 2016. Published online.
41 Jeong SS, Nakamura K, Yoshioka S, Obara Y, Kataoka M. Fracture toughness of granite measured using micro to macro scale specimens. *Procedia Eng*. 2017;191:761–767. https://doi.org/10.1016/j.proeng.2017.05.242.
42 Kataoka M, Obara Y. Size effect in fracture toughness of sandstone. In: *13th ISRM International Congress on Rock Mechanics*. 10–14 May. Canada: Montréal; 2015.
43 Lim IL, Johnston IW, Choi SK, Boland JN. Fracture testing of a soft rock with semi-circular specimens under three-point bending. Part 1—mode I. *Int J Rock Mech Min Sci Geomech Abstr*. 1994;31(3):185–197. https://doi.org/10.1016/0148-9062(94)90463-4.

44 Zhang J, Little DN, Grajales J, You T, Kim Y-R. Use of semicircular bending test and cohesive zone modeling to evaluate fracture resistance of stabilized soils. *Transp Res Rec J Transp Res Board*. 2017;2657(1):67–77. https://doi.org/10.3141/2657-08.

45 Rivera-Perez JJ. *Effect of Specimen Geometry and Test Configuration on the Fracture Process Zone for Asphalt Materials*. 2017. Published online.

46 Martin CD, Chandler NA. The progressive fracture of Lac du Bonnet granite. *Int J Rock Mech Min Sci Geomech Abstr*. 1994;31(6):643–659. https://doi.org/10.1016/0148-9062(94)90005-1.

47 Zhang Q, Duan K, Xiang W, Yuan S, Jiao Y. Direct tensile test on brittle rocks with the newly developed centering apparatus. *Geotech Test J*. 2018;41(1):92–102.

48 Moradian Z, Einstein HH, Ballivy G. Detection of cracking levels in brittle rocks by parametric analysis of the acoustic emission signals. *Rock Mech Rock Eng*. 2016;49(3):785–800. https://doi.org/10.1007/s00603-015-0775-1.

49 Anderson TL. *Fracture Mechanics: Fundamentals and Applications*. third ed. CRC Press; 2005.

50 Şener S, Tutluoglu L. Fracture toughness analysis of Ankara andésite. In: *Proceedings of 18th International Mining Congress and Exhibition of Turkey*. IMCET.; 2003:89–92.

51 Atkinson BK. Subcritical crack growth in geological materials. *J Geophys Res Solid Earth*. 1984;89(B6):4077–4114. https://doi.org/10.1029/JB089iB06p04077.

52 Landis EN, Baillon L. Experiments to relate acoustic emission energy to fracture energy of concrete. *J Eng Mech*. 2002;128(6):698–702. https://doi.org/10.1061/(ASCE)0733-9399(2002)128:6(698).

53 Han QH, Yang G, Xu J. Experimental study on the relationship between acoustic emission energy and fracture energy of crumb rubber concrete. *Struct Contr Health Monit*. 2018;25(10):1–13. https://doi.org/10.1002/stc.2240.